

# Computational Analysis of Rocket-Assisted Projectile Trajectory

Abdellah Ferfour <sup>1)</sup>  
Damir D. Jerković <sup>1)</sup>  
Aleksandar V. Kari <sup>2)</sup>  
Saša Živković <sup>2)</sup>  
Mirko Karić <sup>2)</sup>

A computational analysis was carried out in order to study the effect of solid rocket motor operating parameters on the trajectory elements of 155mm rocket-assisted projectile. Two numerical solutions have been programmed for this purpose. The first for the rocket motor internal ballistic calculation. The second is intended for the six degree-of-freedom (6-DOF) trajectory determination for both unpowered and powered flight. The effect of three operating parameters of the solid rocket motor on the trajectory elements was taken into account, namely: (1) thrust-time profile (neutral, regressive or progressive), (2) working time and (3) ignition delay. The results obtained following this analysis are helpful as a preliminary stage in the design of extended range projectiles in order to optimize flight performance.

*Key words:* rocket-assisted projectile, trajectory elements, internal ballistic calculation, 6-DOF trajectory model.

## Introduction

EXTENDING the range of artillery projectiles is crucial to improve their effectiveness on the battlefield. This expansion helps maintain a strategic advantage to ensure successful operations in different combat scenarios. Projectile range can be extended by many methods, such as increasing muzzle velocity; boosted (rocket-assisted) projectile; or by improved ballistics, including drag reduction or using subcalibers [1]. The rocket-assisted projectile (RAP) is a type of shell that has a small solid propellant rocket motor at the base to extend its range [2]. The rocket motor ignites after a predetermined delay after muzzle exit and operates for a short time to quickly increase projectile velocity (powered flight). After that, the projectile flies as an unpowered artillery shell, achieving greater ranges than the conventional one. Its range depends on its initial velocity and ballistics, and also on the operating parameters of its rocket motor. Hence the need to study the rocket motor operating parameters that could impact the performance of this type of projectile. This constitutes the main purpose of the present work that aims to study the effect of three operating parameters of the solid rocket motor on the trajectory elements of a 155mm rocket-assisted projectile, namely: (1) thrust-time profile (neutral, regressive or progressive), (2) working time and (3) ignition delay. This work is divided into five sections: the second section describes projectile motion model; the third section covers the internal ballistic theory of rocket motor. The fourth section includes the obtained results and their analysis and discussion. Finally, the fifth section contains the main conclusions.

## Projectile motion model

The primary objective of external ballistics is to compute the trajectory of the projectile during its flight. In other words, the prediction of trajectory elements such as velocity, range, altitude, crossrange (deflection), spin, impact angle, etc. This objective is achieved by establishing an appropriate model of projectile motion in the form of a system of differential equations and solving them. The projectile mechanically represents a rigid body whose motion model requires the prior definition of certain physical parameters that determine: the structure of the body, the characteristics of the coordinate system in which the trajectory is considered, the forces acting on the body, the environment properties through which the body moves and the initial conditions of motion [3]. The motion of the projectile with respect to the Earth is relative. The projectile velocity in relation to the Earth denotes its relative velocity, while the time derivatives of its projections onto the axes of any coordinate system constitute the components of the relative acceleration.

The six degree-of-freedom (6-DOF) trajectory model of reference [4] was used for the purposes of determining the trajectory elements of the projectile considered in this study. This model is formulated to solve the projectile pitching and yawing motion in terms of direction cosines of the projectile axis of symmetry, rather than the Eul-angle method used is several other 6-DOF models [4]. Only the starting vector equations of the model are mentioned in this section. The full development of the model leading to the system of differential equations which describe the projectile motion is detailed in

references [4,5]. A right-handed, rectangular coordinate system, with its origin located at the gun muzzle was adopted. In this coordinate system the 1-3 plane is tangent to the earth surface at the launch point, the 1-axis points downrange, the 2-axis points vertically upward through the launch point, and the 3-axis points to the right, when looking downrange. The trajectory and the 6-DOF coordinate system used here are illustrated in Fig.1.

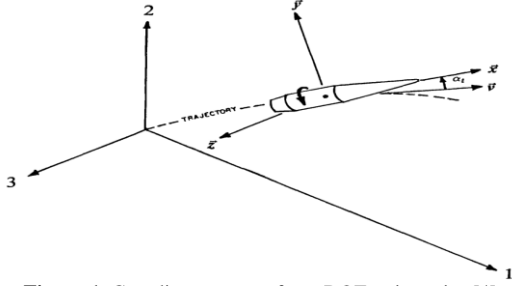


Figure 1. Coordinate system for 6-DOF trajectories [4]

Newton's laws of motion state that the rate of change of linear momentum must equal the sum of all the externally applied forces, and that the rate of change of angular momentum must equal the sum of all the externally applied moments. Newton's laws for a rocket-assisted projectile are:

- Vector equation for the relative motion of the center of gravity (CG) (Fig.2);

$$m \frac{d\vec{V}}{dt} = \sum \vec{R} + m\vec{g} + m\vec{a}_c + \vec{F} \quad (1)$$

- Vector equation of motion about the center of gravity (Fig.2);

$$\frac{d\vec{H}}{dt} = \sum \vec{M}_R + \vec{M}_F \quad (2)$$

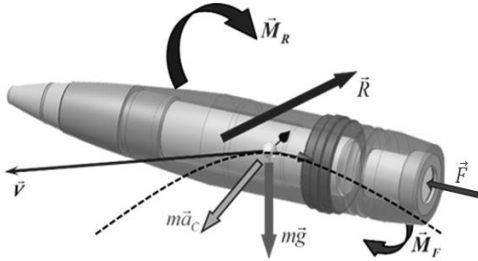


Figure 2. Forces and moments acting on the projectile

Where are:  $m$  projectile mass,  $\vec{V}$  vector velocity with respect to the ground-fixed coordinate axes,  $\sum \vec{R}$  vector sum of all aerodynamic forces,  $\vec{g}$  acceleration due to gravity,  $\vec{a}_c$  Coriolis acceleration due to the earth rotation,  $\vec{F}$  rocket thrust forces,  $\vec{H}$  total vector angular momentum of the projectile,  $\sum \vec{M}_R$  vector sum of all aerodynamic moments (referenced to the CG),  $\vec{M}_F$  rocket thrust moments.

The aerodynamic forces and moments are calculated based on the prior determination of all their static and dynamic aerodynamic coefficients. This can be done via experimental (e.g., wind tunnel, aeroballistics spark facilities, and free-flight ranges) and computational methods, ranging from semi-empirical design codes to full three-dimensional Navier Stokes based computational fluid dynamics (CFD) codes.

### Internal ballistic of rocket motor

All the rocket propulsion systems are explained by

Newton's third law of motion which states that there is always an equal and opposite reaction for every action [6]. Accurate internal ballistic (IB) calculation of solid propellant rocket motor (SPRM) working parameters is very important process, in all design phases [7]. The combustion chamber of the rocket motor (RM) serves as a solid propellant reservoir, in which the chemical energy of the propellant is transformed into the kinetic energy of the combustion products. The chamber with cylindrical section is the most common SPRM case shape [8]. Geometry of propellant grain is various for every rocket motor and also variable during the operating period [7]. The RM operating regime calculation can be conducted using IB coefficients, which represent certain parameters or processes characteristic inherent to RM performance (Fig.3). These coefficients can be derived theoretically, experimentally or semi-empirically.

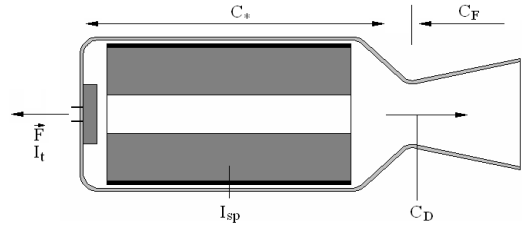


Figure 3. Internal ballistic coefficients and performance parameters scheme [7]

Thrust  $F(t)$  is total produced force by RM, in the axial direction, i.e. along the axis of symmetry of the projectile. It represents the integral of the pressure field acting on both internal and external surfaces of the RM, resulting in the overall reactive force known as thrust.

$$F = \dot{m} \cdot V_e + (p_e - p_a) \cdot A_e \quad (3)$$

Expanding pressure at nozzle exit, with respect to atmospheric pressure, can be differentiated into following flow conditions which depends on the difference  $(p_e - p_a)$  [9]:

- $p_e > p_a$ , under-expanded (the most favored and commonly used);
- $p_e = p_a$ , fully-expanded (adapted nozzle, higher exit velocity);
- $p_e < p_a$ , over-expanded (negative effect, flow detachment).

Where are:  $p_a$  atmospheric pressure,  $p_e$  nozzle exit pressure,  $\dot{m}$  mass flow rate,  $V_e$  nozzle exit velocity,  $A_e$  nozzle exit area.

Total impulse  $I_t$  is the integral of thrust curve over the total operating time period  $\tau$ . It is equivalent of energy amount, released from propellant charge mass. An average thrust  $F_{avg}$  could be taken to calculate the total impulse over the effective working time period  $t_e$ .

$$I_t = \int_0^\tau F(t) \cdot dt \quad (4)$$

$$I_t = F_{avg} \cdot t_e \quad (5)$$

The specific impulse  $I_{sp}$  represents the thrust per unit propellant "weight" flow rate  $\dot{m}$ , i.e. total impulse per one kilogram of propellant mass  $m$  [7,10]. It is an important figure of merit of the performance of any RM [10], which also depends from RM and nozzle geometry design quality [7].

$$I_{sp} = \frac{F}{\dot{m}} = \frac{I_t}{m} \quad (6)$$

The specific impulse  $I_{sp}$  can also be expressed as the ratio between the thrust coefficient  $C_F$  and the discharge coefficient  $C_D$ .

$$I_{sp} = \frac{C_F}{C_D} \quad (7)$$

The thrust coefficient  $C_F$  is dimensionless. It represents efficiency of thrust generation, regarding nozzle flow efficiency [7]. For specific nozzle throat area  $A_t$ , thrust coefficient defines amount of thrust generated from products pressure  $p_c$  in combustion chamber.

$$C_F = \frac{F}{p_c A_t} = \sqrt{\frac{2\kappa^2}{\kappa-1} \left(\frac{2}{\kappa+1}\right)^{\frac{\kappa+1}{\kappa-1}} \left[1 - \left(\frac{p_e}{p_c}\right)^{\frac{\kappa-1}{\kappa}}\right] + \frac{p_e - p_a}{p_c} \frac{A_e}{A_t}} \quad (8)$$

The ratio of the nozzle exit area  $A_e$  to the throat area  $A_t$  is called the nozzle area expansion ratio  $\varepsilon$ , and is given by the equation (8).

$$\varepsilon = \left[ \left(\frac{2}{\kappa+1}\right)^{\frac{1}{\kappa-1}} \cdot \left(\frac{p_c}{p_e}\right)^{\frac{1}{\kappa}} \cdot \left[ \frac{\kappa+1}{\kappa-1} \cdot \left(1 - \left(\frac{p_c}{p_e}\right)^{\frac{1-\kappa}{\kappa}}\right) \right] \right]^{-0.5} \quad (9)$$

Discharge coefficient  $C_D$  is measure of chamber and nozzle flow losses. It defines mass flow rate  $\dot{m}$  through throat area  $A_t$  induced with products pressure energy in chamber [7].

$$C_D = \frac{\dot{m}}{p_c A_t} = \sqrt{\frac{\kappa}{RT_c} \left(\frac{2}{\kappa+1}\right)^{\frac{\kappa+1}{\kappa-1}}} \quad (10)$$

The characteristic velocity  $C^*$  is a function of the propellant characteristics and combustion chamber design, and it is essentially independent of the nozzle characteristics [6,7]. It is defined as the product of chamber pressure  $p_c$  and nozzle throat area  $A_t$  divided by the propellant mass flow rate  $\dot{m}$  [6].

$$C^* = \frac{p_c A_t}{\dot{m}} = \frac{1}{C_D} \quad (11)$$

Where are:  $\kappa$  heat capacity ratio,  $R$  gas constant,  $T_c$  chamber temperature.

In addition to the introduced coefficients and performance parameters, the RM operating regime is heavily influenced by the combustion products properties and combustion characteristics, such as the burning rate  $r$  [7]. The RM propellant grain burning regresses in a perpendicular way to the surface which characterizes the grain combustion [6]. The burning rate as a function of chamber pressure  $p_c$  could be determined for different types of propellants using empirical Saint Robert or Vieille law for a given burning rate coefficient  $b$  and pressure exponent  $n$ .

$$r = b \cdot p_c^n \quad (12)$$

The design of a SPRM typically starts with establishing the technical and tactical requirements that it must satisfy. The type of propellant can be selected, based on desired performances and special requirements [11].

The pressure change in the combustion chamber can be calculated using the mass conservation equation. Total pressure within the combustion chamber is nearly uniform across the entire free volume at certain moments. This pressure level can be determined based on products mass balance, accounting for generation, accumulation and discharging through nozzle. The production of products on

burning surfaces equals the change in mass of the combustion products within the chamber and discharged through the nozzle throat [7].

For unsteady flow through the RM domain (Fig.4), continuity equation has the following form:

$$\dot{m}_b(t) = \dot{m}_c(t) + \dot{m}_t(t) \quad (13)$$

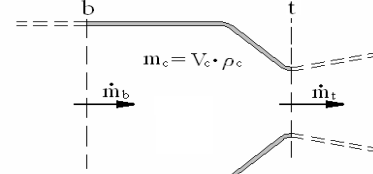


Figure 4. Combustion products mass balance in RM flow

Domain [7]

The mass balance equation can be expressed as first order differential equation of unknown variable chamber pressure, which is nonlinear and inhomogeneous. The details of this equation extraction can be found in [12]. Nonlinearity of this ordinary differential equation manifests in the burning rate function, which dependent from chamber pressure. Some functions are defined in terms of the burned web  $x(t)$ , such as the burning area  $A_b(t)$  and the chamber free volume  $V_c(t)$ . Burned web is also function of time, and can be derived from burning rate function. Those dependences can be written in form of system of two differential equations, one integral and two algebraic equations (equations 14-18). Solving this system we can obtain pressure-time and burned web-time curves.

$$A_b(t) = A_b[x(t)] \quad (14)$$

$$V_c(t) = V_c(t=0) + \int_0^t A_b[x(t)] \cdot r(t) \cdot dt \quad (15)$$

$$r(p_c, t) = r[p_c(t)] \quad (16)$$

$$\frac{d}{dt} p_c(t) = \frac{R \cdot T_c \cdot A_b(t) \cdot r(p_c, t) \cdot \rho_p}{V_c(t)} - \quad (17)$$

$$\varphi \cdot \frac{A_t}{V_c(t)} \cdot \sqrt{\kappa \cdot R \cdot T_c \cdot \left(\frac{2}{\kappa+1}\right)^{\frac{\kappa+1}{\kappa-1}} \cdot p_c(t)} - \frac{A_b(t) \cdot r(p_c, t) \cdot p_c(t)}{V_c(t)}$$

$$\frac{d}{dt} x(t) = r(p_c, t) \quad (18)$$

Using calculated real  $C_F$  and pressure-time curve, thrust-time curve can be also calculated, according to equation:

$$F(t) = C_F \cdot p_c(t) \cdot A_t \quad (19)$$

Where are:  $\rho_p$  propellant density,  $\varphi$  throat coefficient.

## Results and discussions

### Research model

The 155 mm rocket assisted projectile (RAP), shown in Fig.5, was chosen as the research model in this work. The projectile has the following characteristics: reference diameter (cal.) 155mm, total length ~ 5.61 cal., nose length ~ 3.37 cal., boattail length ~ 0.55 cal., center of gravity (CG) from nose ~ 3.53 cal., explosive charge mass ~ 7 kg, rocket motor

propellant mass  $\sim 3$  kg and projectile mass  $\sim 43$  kg.

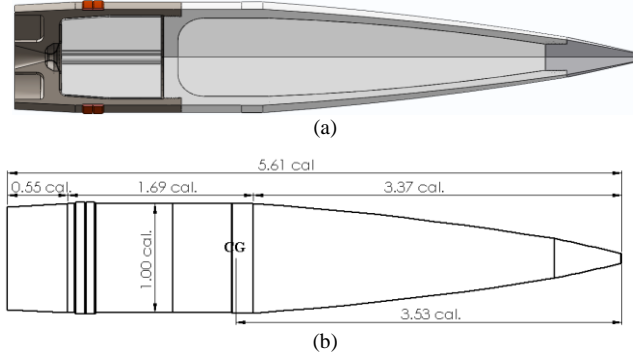


**Figure 5.** Projectile model, (a) CAD model, (b) dimensions in cal.

This projectile fired from 39 calibre howitzer with 19 litre chamber volume, should reach velocity of 830 m/s at the muzzle exit. The solid rocket motor, placed at the rear, must be ignited in the ascending part of the ballistic trajectory, after a predetermined ignition delay, and with a short working time, to quickly increase projectile velocity.

#### Rocket motor internal ballistic calculation

The aim of the internal ballistic calculation is to determine the thrust-time variation of the solid rocket motor, which is subsequently used in the 6-DOF projectile motion model. Hence, this section does not include the presentation of all the outcomes from the intermediate stages of the calculation. The required propellant solid rocket motor characteristics are: total impulse  $\sim 6500$  Ns, propellant mass  $\sim 3$  kg and effective working time which takes values between 2s and 4s with a step of 0.5s, in order to analyze its effect on the projectile range. Table 1 specifies the necessary input data for the calculation.

**Table 1.** Input data for the internal ballistic calculation

Input data	Value
Temperature of combustion $T_c$	2900 [K]
Mean chamber pressure $p_{cm}$	200 [bar]
Propellant density $\rho_p$	1750 [kg/m <sup>3</sup> ]
Specific heat ratio $\kappa$	1.25 [1]
Gas constant $R$	308.7 [J/kg·K]

Three distinct propellant grain configurations are selected (star, slot and tubular), as shown in Fig.6, to achieve the desired thrust-time profiles (neutral, regressive and progressive). The star configuration is inhibited at outer diameter and rear-end. The slot and tubular configurations are inhibited at entire outer surface. The burning area variations versus burning web for the three grain configurations are shown in Fig.7, labeled as follows: N (neutral), R (regressive) and P (progressive).

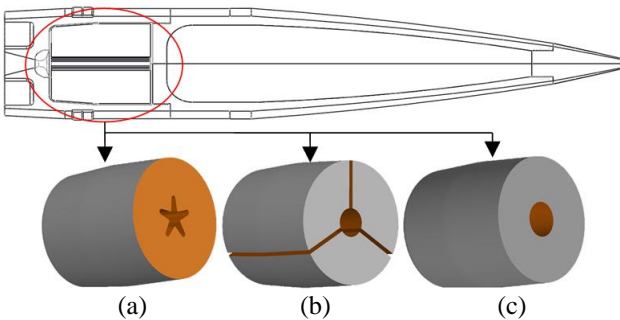


**Figure 6.** Propellant grain configurations, (a) star (neutral), (b) slot (regressive), (c) tubular (progressive)

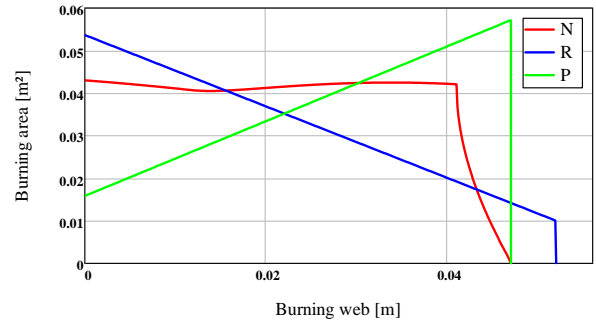


**Figure 7.** Burning area variations versus burning web for the three grain configurations

After having obtained the burning area variations as a function of the burning web, it is possible to compute the pressure-time evolution  $p_c(t)$  in combustion chamber by solving the system of equations (14-18), which is composed of two differential equations, one integral and two algebraic equations. The differential equations were numerically integrated using the 4th-order Runge-Kutta method. In order to determine the thrust force of the rocket motor over time using equation (19), it is also essential to calculate the thrust coefficient  $C_F$  defined by equation (8). Thus, the nozzle exit pressure  $p_e$  must be determined by utilizing equation (9), which describes the nozzle area expansion ratio  $\epsilon$ , taking into account the atmospheric pressure  $p_a$  which corresponds to the altitude at which the rocket motor ignites. The obtained thrust-time curves for an effective working time of 3s, calculated for the three grain configurations using equation (19), are shown in Fig.8.

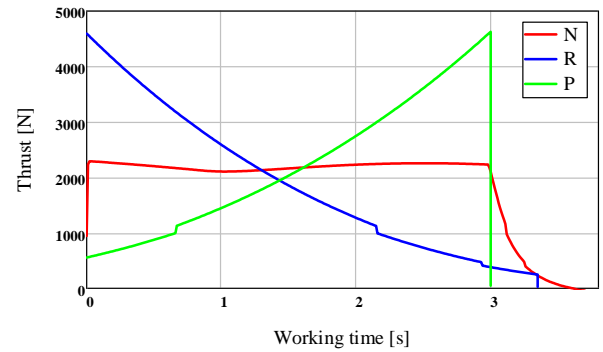


**Figure 8.** Thrust-time variations for the three grain configurations

The thrust-time curves were also calculated for the three cases of grain configuration considering other effective working times, as illustrated in Fig.9 for the neutral thrust profile. This was done to analyze the effect of this operating parameter on the range of the projectile.

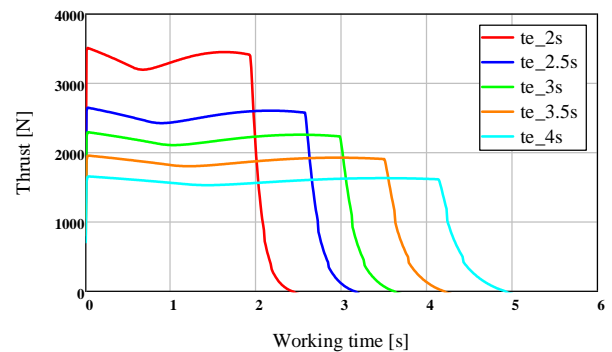


**Figure 9.** Thrust-time variations for different effective working times (neutral profile)

### Analysis of trajectory elements

As mentioned before, the six degrees of freedom (6-DOF) trajectory model is used in this work for the purpose of determining the projectile trajectory elements. A 6-DOF trajectory program was built in OCTAVE software to implement the 6-DOF trajectory model, following the algorithm presented in the Fig.10. This program is designed to perform external ballistic calculation and flight simulation for a rigid, rotationally symmetric projectile, acted on by all significant aerodynamic forces and moments, in addition to wind, gravity, Coriolis forces and rocket thrust. This program also includes an improved semi-empirical method for power-on base-drag prediction during rocket motor operating phase, developed by [13]. The differential equations of projectile motion were numerically integrated using the 4th-order Runge-Kutta method.

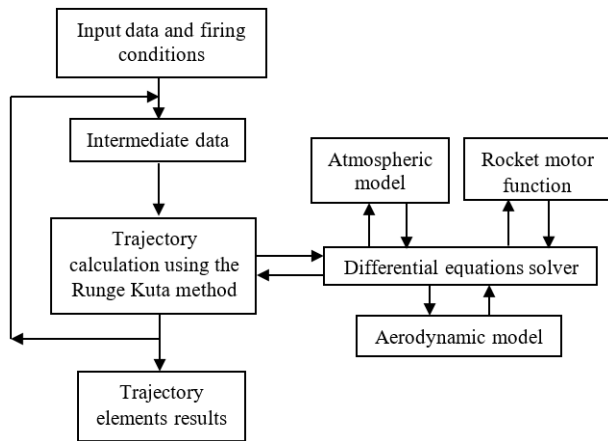


Figure 10. Numerical solution program algorithm

The atmospheric model is included to determine variations in air temperature, speed of sound and air density as a function of flight altitude, according to the ANA standard atmosphere [3]. The static and dynamic coefficients of aerodynamic forces and moments are determined via semi-empirical design codes (ADK0, ADK1 and ADK2), using aerodynamic prediction based on theories of reference [14-16]. The effect of wind velocity components was not included in the calculation of projectile trajectory elements.

To check the accuracy of the 6-DOF program, an existing projectile case was considered. This concerns the M101 155mm artillery projectile. The projectile input data and firing conditions are presented in Table 2. The comparison between the firing-tables data and results obtained by numerical calculation are illustrated in Table 3.

Table 2. Input data and firing conditions of the M101 projectile

Projectile input data	
Caliber $d$ [mm]	155
Length $l$ [mm]	704
Mass $m$ [kg]	43.25
Center of gravity from nose $x_{CG}$ [mm]	458.37
Moments of Inertia [kg·m <sup>2</sup> ]	
Axial $I_{xx}$	0.144
Lateral $I_{yy} = I_{zz}$	1.216
Firing conditions	
Muzzle velocity $V_0$ [m/s]	840
Firing altitude $Y_0$ [m]	500
Muzzle spin rate $p_0$ [rad/s]	1162
Firing elevation angle $\theta_0$ [°]	47.88

Table 3. Trajectory elements of the M101 projectile

	6-DOF calculation	Firing Tables data	Deviation [%]
Summit $Y_{max}$ [m]	9260	8963	+3.3
Range $X_{max}$ [m]	23532	23808	-1.2
Crossrange $Z_{max}$ [m]	911.6	982.3	-7.2
Impact angle $\theta_f$ [°]	65.68	65.03	+0.9
Impact time $t_f$ [s]	85.77	85	+0.9
Impact velocity $V_f$ [m/s]	337.3	337	+0.1

In Table 3, it can be seen that the percent deviations between the calculated results and firing-tables data are not significant, which confirms the accuracy of the 6-DOF program as a tool for predicting trajectory elements.

Once the program accuracy has been checked, it becomes feasible to investigate the effect of the solid rocket motor operating parameters on the trajectory elements of the 155mm rocket-assisted projectile (RAP), especially their effect on the projectile range. As mentioned before, these parameters are: (1) thrust-time profile (neutral, regressive and progressive), (2) working time and (3) ignition delay. The input data and firing conditions of the studied projectile are presented in Table 4.

Table 4. Input data and firing conditions of the rocket-assisted projectile

Projectile input data		
Caliber $d$ [mm]		155
Length $l$ [mm]		870
Before burnout	Mass $m_i$ [kg]	43
	Center of gravity from nose $x_{CGi}$ [mm]	548.7
	Axial Moment of Inertia $I_{xxi}$ [kg·m <sup>2</sup> ]	0.14
	Lateral Moment of Inertia $I_{yyi} = I_{zxi}$ [kg·m <sup>2</sup> ]	1.78
After burnout	Mass $m_f$ [kg]	40
	Center of gravity from nose $x_{CGf}$ [mm]	540
	Axial Moment of Inertia $I_{xxf}$ [kg·m <sup>2</sup> ]	0.13
	Lateral Moment of Inertia $I_{yyf} = I_{zxf}$ [kg·m <sup>2</sup> ]	1.67
Firing conditions		
Muzzle velocity $V_0$ [m/s]		830
Firing altitude $Y_0$ [m] (sea level)		0
Muzzle spin rate $p_0$ [rad/s]		1148
Firing elevation angle $\theta_0$ [°]		Variable

Figure 11 shows the projectile range changes versus firing angle, for each of the three thrust-time profiles, with working time of 3s and ignition delay of 7s. The projectile range, as indicated in the Fig.11, changes with the thrust-time profile. For this configuration, the maximum range is achieved at a firing angle of 55° in the three profile cases with different values, while the neutral profile exhibiting the largest.

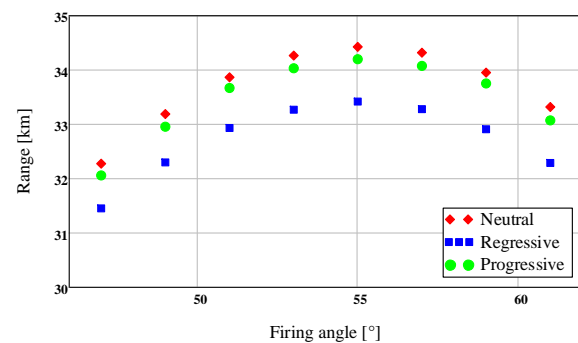


Figure 11. Projectile range changes versus firing angle (working time 3s, ignition delay 7s)

Altitude and crossrange versus range are shown in Figs. 12 and 13 for unpowered and powered flights (for each of the three thrust-time profiles), with working time of 3s, ignition delay of 7s and firing angle of 55°. These two Figs. 12 and 13

indicate that this trajectory parameters for powered flight exhibit the same variation patterns as those for unpowered flight. The trajectory does not have a symmetry axis that passes through its summit, which is due to the impact of total aerodynamic load on projectile motion. Compared to unpowered flight, Fig.12 illustrates the benefit of using the rocket motor to enhance the performance of artillery projectiles, with extensions of more than 35% for range and around 25% for summit altitude.

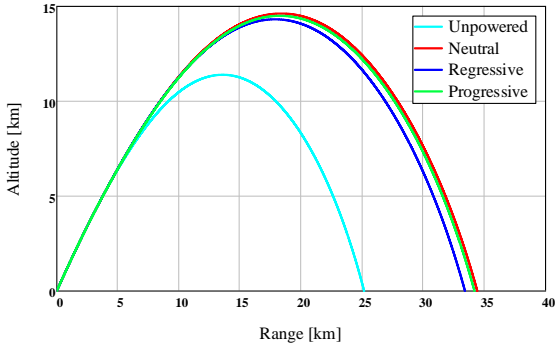


Figure 12. Altitude versus range (working time 3s, ignition delay 7s and firing angle 55°)

The projectile deflection (crossrange) in the horizontal plan, shown in Fig.13, is caused by the Magnus effect. For uncontrolled flight, this deflection expands as the projectile range increases.

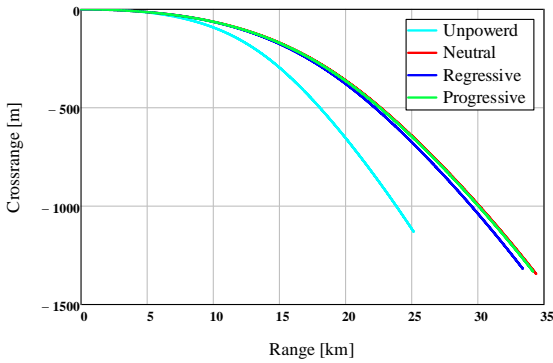


Figure 13. Crossrange versus range (working time 3s, ignition delay 7s and firing angle 55°)

Figure 14 illustrates the flight velocity versus flight time from launch to impact point for unpowered and powered flights (neutral, regressive and progressive), with working time of 3s, ignition delay of 7s and firing angle of 55°.

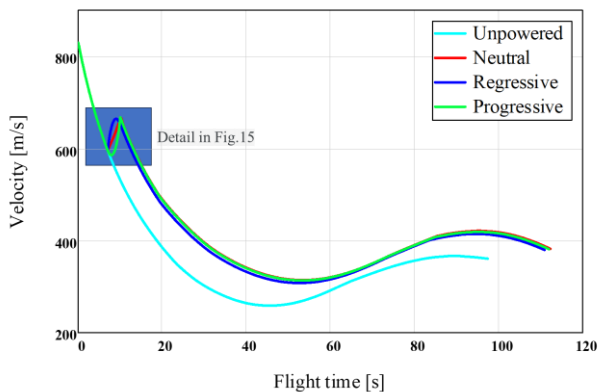


Figure 14. Flight velocity versus flight time (working time 3s, ignition delay 7s and firing angle 55°)

As depicted in Fig.14, it can be seen that the velocity decreases immediately after launch due the impact of total aerodynamic load. During rocket motor operating phase, which begins 7 seconds after launch continues for 3 seconds, the velocity quickly increases due to the thrust force. Following that, it begins to decrease again under the same aerodynamic impact until the projectile reaches the highest point of the trajectory, which is the summit point. At that highest point, the vertical velocity component becomes zero. After this, the velocity increases again under the influence of gravitational acceleration. Fig. 14 further shows that the RAP projectile velocity at both the summit and impact points, as well as the total flight time, exceed those of the unassisted projectile (unpowered flight).

Velocity-time variations during rocket motor operating phase are shown in Fig.15, for each of the three thrust-time profiles, with working time 3s, ignition delay 7s and firing angle 55°.

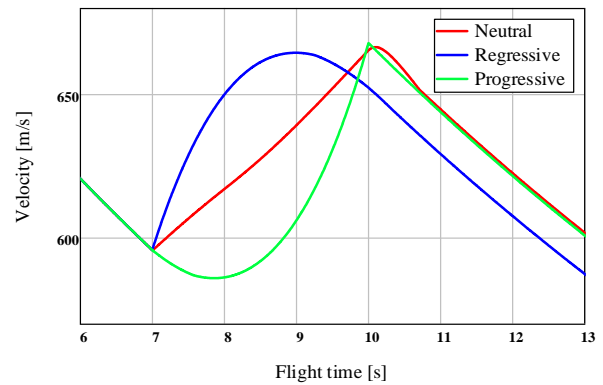
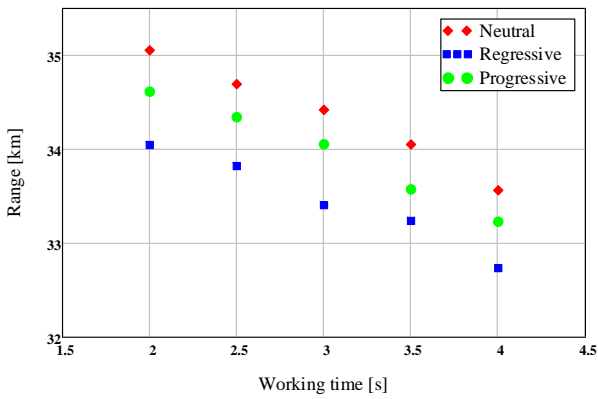


Figure 15. Velocity-time variations during rocket motor operating phase (working time 3s, ignition delay 7s and firing angle 55°)

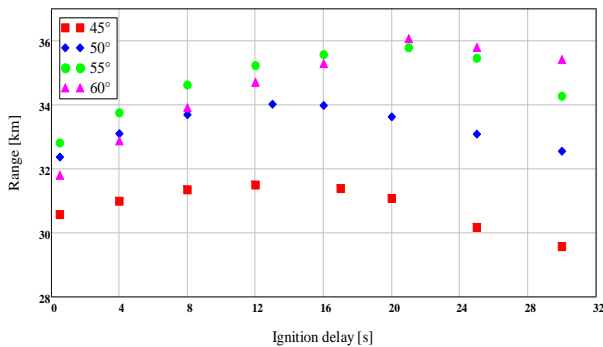
It is evident from Fig.15 that the velocity-time profiles reflect the integrated form of the thrust-time profiles. In the case of neutral thrust, the integration produces a linear velocity-time profile, showing a steady rate of velocity change. Concerning the case of regressive thrust which decreases with time, the integration gives a concave-down parabolic curve, indicating a decelerating rate of velocity increase. Finally, and for the progressive thrust that increases with time, the integration produces a concave-up parabolic curve, indicating an accelerating rate of velocity increase. These variations highlight the effects of the different thrust-time profiles on the projectile velocity.

Figure 16 shows the projectile range changes versus working time, for each of the three thrust-time profiles, with ignition delay of 7s and firing angle of 55°. The projectile range varies not only with the thrust-time profile, but also with the working time, where the range extension increases by using shorter working time, as shown in Fig.16. The maximum range for this configuration is reached at a working time of 2s in all three profile cases, each with distinct values, while the neutral profile shows the largest range. However, using shorter working times while maintaining the required total impulse leads to high thrust levels (as already shown in the Fig.9 for the neutral profile), which demands careful consideration of the effects of thrust on the projectile aerodynamic characteristics.



**Figure 16.** Projectile range changes versus working time (ignition delay 7s and firing angle 55°)

After illustrating the effect of the thrust-time profiles and working time on the trajectory elements, especially the projectile range, it remains to analyze the effect of the rocket motor ignition delay. This was done with working time of 3s and neutral thrust-time profile, as this profile has shown to be more effective than the other two profiles.



**Figure 17.** Projectile range changes versus ignition delay for different firing angles (neutral thrust profile, working time 3s)

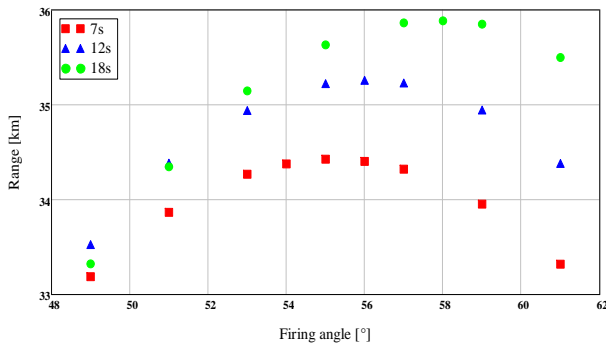


**Figure 18.** Projectile range changes versus firing angles for different ignition delays (neutral thrust profile, working time 3s)

Projectile range changes versus ignition delay for different firing angles are shown in Fig.17. The outcomes of this figure illustrate that the range varies with the ignition delay, and the projectile maximum range for each firing angle is associated with particular ignition delay. Fig.18 shows the projectile range changes versus firing angle for different ignition delays. Fig.18 also illustrates that the firing angle corresponding to the maximum range changes with the ignition delay.

## Conclusion

In this work, computational analysis was performed to examine the influence of different operating parameters of solid rocket motor on the trajectory elements of 155mm rocket-assisted projectile, especially the projectile range. The

six degree-of-freedom trajectory model and the solid rocket motor internal ballistic have been briefly explained. The selected operating parameters of solid rocket motor for this analysis are: (1) thrust-time profile, (2) working time and (3) ignition delay. Thrust-time variations of three selected propellant grain configurations (star, slot and tubular) were computed, in order to obtain the desired thrust-time profiles (neutral, regressive and progressive). The trajectory elements were calculated using a 6-DOF trajectory program, built for the purpose of this work.

The 6-DOF program results showed that the trajectory elements of rocket-assisted projectile are impacted not only by the projectile characteristics and firing conditions, but also by the operating parameters of the solid rocket motor. The results also illustrated the benefit of using the solid rocket motor, with extensions of more than 35% for range and around 25% for summit altitude, and with longer time of flight. Among the three thrust time profiles considered for this analysis, the neutral one enabled more range extension, with slight differences compared to the progressive profile. It has also been shown that the range extension increases using shorter working times, but with high thrust levels. Concerning the ignition delay, the results illustrated that the projectile range varies with this operating parameter. It was found that the projectile maximum range for each firing angle is related to a specific ignition delay.

For possible perspectives, this work can be extended to investigate the incorporation of base bleed unit and solid rocket motor in the same artillery projectile, wherein each is used in its most effective part of the ballistic trajectory.

## Acknowledgement

This research has been supported by the University of Defence in Belgrade within the Project No. VA/TT/1/24-26.

## References

- [1] Gunnars N. E., Andersson K. and Hellgren R., Base-Bleed Systems for Gun Projectiles, Gun Propulsion Technology, vol. 109, p. 537–562, 1988.
- [2] Guodong Z., The Study of the Modeling simulation for the Rocket-Assisted Cartridge, IOP Conference Series Materials Science and Engineering, vol. 439(4), 2018.
- [3] Regodić D., Spoljna balistika, Beograd, Vojna Akademija, 2006.
- [4] McCoy R. L., Modern Exterior Ballistics, Schiffir Publishing Ltd, ISBN: 978-0-7643-3825-0, 1998.
- [5] Carlucci D. E. and Jacobson S. S., Ballistics: Theory and design of guns and ammunition, Florida, United States: CRC Press, 2008.
- [6] Alazeezi M., Design and Optimization of Dual-Propellant Grains of Solid Rocket Motors, University of Belgrade – Faculty of Mechanical Engineering, 2024.
- [7] Živković S., Filipović M., Elek P., Milinović M., Gligorijević N. and Boulahlib M. A., Experimental determination of rocket motor internal ballistic coefficients and performance parameters, in 6th International scientific conference on defensive technologies OTEH, Belgrade, 2014.
- [8] Živković S., Savković M. and Grigorijević N., Solid propellant rocket motor components initial design, chez 4th International scientific conference on defensive technologies OTEH, Belgrade, 2011.
- [9] Jelić Z., Optimization of design parameters for modular range enhanced projectile, Cranfield University, Cranfield Defence and Security, Doctoral Dissertation, 2015.
- [10] George P. S. and Donald M. R., Rocket Propulsion Element, Hoboken, New Jersey, John Wiley & Sons, Inc., 2017.
- [11] Ockoljić G., Živković S. and Subotić S., Aerodynamic coefficients determination for antitank missile with lateral jets, in 4th International scientific conference on defensive technologies OTEH, Belgrade, 2011.
- [12] Marjanović G., Živković S. and Gligorijević N., Program SVOD for Solid Propellant Grain Design, in 5th International scientific

- conference on defensive technologies OTEH, Belgrade, 2012.
- [13] Moore F. G. and Moore L. Y., Improvements to Power-On Base Pressure Prediction for the Aeroprediction Code, *Journal of Spacecraft and Rockets*, vol. 47(1), pp. 101-112, 2010.
- [14] Regodić D., *Zbirka rešenjih zadataka iz spoljne balistike*, Beograd: Vojna Akademija, 2003.
- [15] Jerković D. and Samardžić M., The aerodynamic characteristics determination of classic symmetric projectile, in the 5th international symposium about design in mechanical engineering KOD, Novi Sad, 2008.
- [16] Ferfour A., Allouche T., Jerković D., Hristov N., Vučković M. and Benmeddah A., Prediction of drag aerodynamic coefficient of the 155mm projectile under axisymmetric flow using different approaches, *Journal of the Serbian Society for Computational Mechanics*, vol. 17(2), pp. 69-86, 2023.

Received: 01.07.2024.

Accepted: 10.09.2024.

## Numerička analiza putanje aktivno-reaktivnog projektila

Numerička analiza je sprovedena kako bi se proučio uticaj radnih parametara raketnog motora sa čvrstim gorivom na elemente putanje aktivno-reaktivnog projektila kalibra 155 mm. Primenjena su dva numerička modela za potrebe proračuna pogona i kretanja. Prvi model se odnosi na proračun unutrašnjebalističkih parametara raketnog motora. Drugi model sa šest stepeni slobode (6-DOF) je korišćen za određivanje elemenata putanje, za faze leta bez pogona i sa pogonom raketnog motora. Uzeta su u obzir tri radna parametra raketnog motora koja utiču na elemente putanje: (1) profil sile potiska (neutralan, degresivan i progresivan), (2) vreme rada i (3) vreme aktiviranja raketnog motora. Rezultati dobijeni ovom analizom korisni su u preliminarnoj fazi projektovanja projektila velikog dometa u cilju optimizacije performansi leta.

*Ključne reči:* aktivno-reaktivni projektil, Elementi putanje, Proračun unutrašnjebalističkih parametara, Model putanje sa šest stepeni slobode kretanja.